frontiers | Frontiers in Materials

TYPE Original Research
PUBLISHED 04 July 2024
DOI 10.3389/fmats.2024.1426979



OPEN ACCESS

EDITED BY
João Reis,
Fluminense Federal University, Brazil

REVIEWED BY
Grzegorz Golewski,
Lublin University of Technology, Poland
Mahmood Ahmad,
University of Engineering and Technology, Peshawar, Pakistan
Nahla Hilal,
University of Fallujah, Iraq

*CORRESPONDENCE
Jinjin Ge,
jge2@foxmail.com

RECEIVED 02 May 2024
ACCEPTED 14 June 2024
PUBLISHED 04 July 2024

CITATION
Ge J, Mubiana G, Gao X, Xiao Y and Du S (2024), Research on static mechanical properties of high-performance rubber concrete.
*Front. Mater.* 11:1426979.
doi: 10.3389/fmats.2024.1426979



# Research on static mechanical properties of high-performance rubber concrete

Jinjin Ge[1,2]*, Gilbert Mubiana[1], Xiaoyu Gao[1], Yunfei Xiao[1] and Suyong Du[1]

[1]School of Civil Engineering and Architecture, Anhui University of Science and Technology, Huainan, China, [2]State Key Laboratory of Mining Responses and Disaster Prevention and Control in Deep Coal Mines, Anhui University of Science and Technology, Huainan, China

High performance concrete (HPC) has the characteristics of high strength, high brittleness and low toughness, so it can not be widely used in engineering field. The rubber particles themselves have good elasticity and excellent wear resistance. To this end, rubber particles were used to prepare high performance rubber concrete (HPRC) instead of fine aggregate, and compressive strength and splitting tensile strength tests were carried out according to standard test methods. These data were evaluated, and it was found that adding different mesh number (10 mesh, 20 mesh, 30 mesh) and different content (10%, 20%, 30%) of rubber particles reduced the compressive and tensile properties of high-performance rubber concrete to different degrees. The rubber particles with l size of 30 mesh and content of 10% have the least influence on the mechanical properties of high-performance rubber concrete, and the compressive strength and tensile strength of HPC 28 days only decrease by 18.19% and 5.56%, respectively. From the damage form, the addition of rubber particles makes the high performance concrete change from brittle to ductile. The research shows that recycling rubber from waste tires into concrete manufacturing is an environmentally friendly and feasible waste management strategy. These results have the potential to replace concrete in construction and promote sustainable growth.

KEYWORDS

**high-performance concrete, rubber particles, rubber concrete, compressive strength, splitting tensile strength**

## 1 Introduction

China's extensive road network primarily consists of asphalt concrete, yet sustained heavy loads and prolonged exposure to high temperatures render these roads susceptible to deformation and deterioration. The repeated stress from vehicular traffic often leads to surface defects and structural ailments. Moreover, the depletion of asphalt as a non-renewable resource further exacerbates the challenge of meeting the nation's growing infrastructure demands. In response, there has been a shift towards utilizing cement concrete for road construction due to its inherent high strength.

The development of modern concrete began in the 18th century with the invention of Portland cement by Joseph Aspdin in 1824. Today, concrete is the most widely used man-made material in the world (Li et al., 2023; Luo et al., 2024), and research continues to improve its properties and sustainability (Lu et al., 2019; Huang et al., 2021a; Huang et al.,

2022; Lu et al., 2023). There are a lot of new research directions in this topic leading towards assessing fracture toughness and fracture processes in concrete composites based on cement matrix including additives or admixtures (Golewski, 2023a; Golewski, 2023b; Golewski, 2023c; Golewski, 2023d; Golewski, 2024a; Golewski, 2024b). These materials can effectively reduce the susceptibility of concrete to cracking (Huang et al., 2021b; Cui et al., 2024). Moreover, the phenomenon of cracking in concrete structures can also be discussed (Long et al., 2023; Wei et al., 2023; Yao et al., 2023; Cao et al., 2024).

However, cement concrete presents its own set of challenges. Under heavy loads and overloading conditions, issues such as plate breakage and surface fragmentation can compromise road safety and longevity. Addressing these concerns is imperative for ensuring the sustainability and resilience of China's road infrastructure amidst increasing transportation demands.

Rubber concrete, an innovative building material emerging in recent years, utilizes treated waste tires to supply rubber pellets for concrete mixtures. It is found that the addition of rubber particles results in lightweight structures with reduced mechanical strength but having higher energy dissipation capacity, thermal resistance, and sound absorption capability (Bala and Gupta, 2021; He et al., 2023; Mohseni and Koushkbaghi, 2023; Singaravel et al., 2024). Siahkouhi et al. (2022) investigated the application of waste rubber and glass materials in the design of concrete railway sleeper mixtures. It was found that the performance of glass powder concrete is better than that of rubber concrete, but lower than the reference sample. Zhang et al. (2023) effectively improved the crack resistance of concrete by adding rubber powder and polypropylene fibers. Sambucci et al. (2020) investigated the effects of sand GTR particles (rubber powder and rubber particles) substitution on material durability and printability of fresh materials. The research results indicate that GTR fillers do not alter the rheological properties of cement materials, promote good compaction of the mixture, hinder crack propagation, reduce permeability porosity, improve surface hydrophobicity, and maintain optimal permeability. Al Osta et al. (2022) investigated the use of recycled high-density polyethylene (HDPE) and debris tires to improve concrete performance. The results showed that when HDPE and crushed rubber (Ru) were used as substitutes for aggregates, the thermal conductivity decreased by about 40%. Although the use of these materials reduces the strength of ordinary concrete, it improves its ductility performance. Furthermore, researchers have explored surface modification techniques for rubber particles to enhance the mechanical properties and abrasion resistance of concrete materials (Roychand et al., 2021; Shahzad and Zhao, 2022; Agrawal et al., 2023; Agrawal et al., 2023; Valente et al., 2023). These modifications aim to improve surface hydrophilicity and enhance the interfacial bonding strength between the cementitious material matrix and rubber particles. In addition to that, researchers have undertaken various explorations aimed at enhancing the mechanical properties of rubber concrete (Sambucci et al., 2020; Juveria et al., 2023; Medina et al., 2023; Wang and Pang, 2023; Youssf et al., 2023).

Research conducted both domestically and internationally indicates that the incorporation of rubber aggregates into concrete formulations often leads to a notable reduction in compressive strength. While this modification enhances material toughness and flexural strength, it remains insufficient to withstand the increasing loads imposed by heavy-duty and overloaded vehicles. Therefore, there is a critical need to develop high-strength and resilient highway rubber concrete capable of accommodating large traffic volumes.

With the aim of advancing the understanding and potential applications of high-performance rubber concrete, this study builds upon experimental investigations conducted on high-performance concrete. Specifically, rubber concrete samples were prepared by replacing river sand with rubber particles of 10 mesh, 20 mesh, and 30 mesh sizes at equal volumes, employing a water-cement ratio of 0.5. Through indoor static testing, the mechanical properties of the samples were rigorously analyzed, focusing on the influence of rubber particle size and dosage on the mechanical characteristics of high-performance concrete. The study systematically evaluates the optimal incorporation amount and particle size of rubber, aiming to ascertain their efficacy in enhancing concrete compressive strength and their suitability for practical engineering applications. Additionally, the study holds practical significance in addressing waste disposal challenges and reducing China's reliance on conventional resources, thereby contributing to sustainable construction practices and resource conservation efforts.

# 2 Materials and sample preparation

## 2.1 Materials

High-performance rubber concrete (HPRC) is composed of cement, silica fume, fly ash, rubber particles, river sand, water reducing agent, water. The main materials used in this study are as follows. 1) Cement: P.II52.5 cement, provided by Anhui Conch Cement Co. Ltd., conforming to astm C150/C150-16E1 (2016) with a specific gravity (SG) of 3.15, its chemical compositions are shown in Table 1. 2) Silica fume: Elkem940 silica fume with 96.3% $SiO_2$ content, its chemical compositions are shown in Table 1. 3) Fly ash: Class C fly ash (particle size 1,000 mesh), its chemical composition is shown in Table 1. 4) River sand: the grading meets the requirements and the fineness modulus is 2.66. 5) Rubber powder: particle size 10 mesh, 20 mesh, 30 mesh, produced by Sichuan Huayi Co. Ltd., as shown in Figure 1. 6) Superplasticizer: water reducing rate 30%, provided by Inshine New Material Technology Co., Ltd.

## 2.2 Sample preparation

More attention is paid on the effect of rubber particle size and content in HPC instead of the behavior of HPC herein. This study focused on the influence of rubber powder on the static mechanical properties of HPC. Therefore, based on the existing mix ratio of HPC, HPRC is prepared by replacing part of river sand with rubber powder. The HPC and HPRC were prepared according to the mixing ratio shown in Table 2.

According to the test mix ratio, the required materials (cement, silica ash, fly ash, rubber particles, river sand) are weighed first, and then the weighed materials are poured into the forced mixer for dry mixing for 3 min. In order to make the materials wrap each other more evenly, the ash knife is used to assist mixing along the inner wall of the mixer during dry mixing. Finally the mixed liquid with water and all water reducer is slowly poured into the mixing pot, at

TABLE 1 Chemical composition of cement, fly ash and silica fume (%).

| Raw material | CaO | $SiO_2$ | $Al_2O_3$ | MgO | $Fe_2O_3$ | $Na_2O$ | $TiO_2$ | $K_2O$ | $SO_3$ |
|---|---|---|---|---|---|---|---|---|---|
| Cement | 62.4 | 22.9 | 5.30 | 1.7 | 3.9 | 0.2 | — | 0.6 | 3 |
| Fly ash | 3 | 57.0 | 25.5 | 0.7 | 4.2 | — | 1.8 | 1.3 | 0.6 |
| Silica fume | 0.6 | 96.3 | 1.1 | 0.4 | 0.5 | 0.9 | — | — | 0.2 |

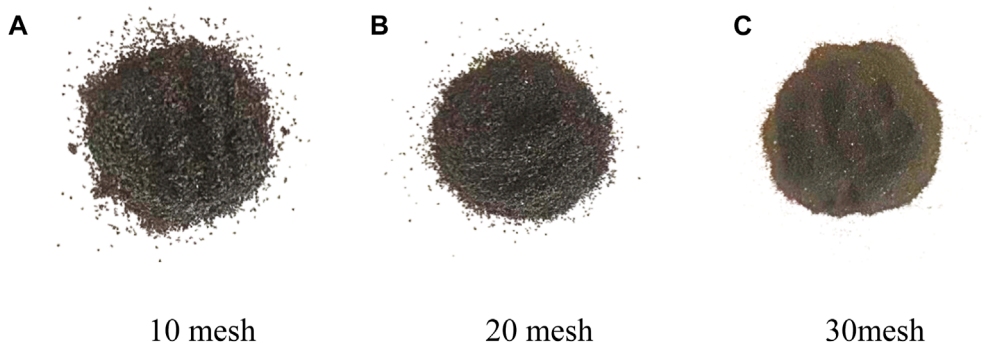


FIGURE 1
The images of using rubber.

TABLE 2 Mix ratio of materials (kg/m$^3$).

| Material | Cement | Silica fume | Fly ash | River sand | Water | Water reducer | Rubber powder | | |
|---|---|---|---|---|---|---|---|---|---|
| | | | | | | | 10-mesh | 20-mesh | 30-mesh |
| HPC | 924.0 | 176.0 | 150.0 | 997.0 | 186.0 | 20.0 | 0 | 0 | 0 |
| HPRC/10% | 924.0 | 176.0 | 150.0 | 897.3 | 186.0 | 20.0 | 26.7 | 27 | 27.1 |
| HPRC/20% | 924.0 | 176.0 | 150.0 | 797.6 | 186.0 | 20.0 | 53.3 | 54 | 54.2 |
| HPRC/30% | 924.0 | 176.0 | 150.0 | 697.9 | 186.0 | 20.0 | 80.0 | 81 | 81.3 |

this time in order to make the water reducer fully contact with the material and play its water reduction performance, the wet mixing time is increased to 6 min. After forming, the specimen was placed on the vibration table for 2 min, and its surface was smoothed with a shovel. Finally, the surface was covered with plastic wrap to prevent moisture loss during maintenance. The above samples of HPC and HPRC were demoulded after 1 day of casting, followed by a standard curing for 3, 7, 28 days.

## 3 Experimental program and methods

According to the test requirements, the specimens with two sizes were prepared. One size is 50 mm × 50 mm × 50 mm what is used for uniaxial compression test, and the other size is Ø 50 mm × 25 mm that is used for Brazilian disc tensile test. In order to analyze the influence mechanism of rubber powder on mechanical properties of HPC, a sample with a volume of about 1 cm$^2$ was extracted from the damaged concrete section, and the hydration was terminated with anhydrous ethanol after the sample was taken out. The sample was then studied using scanning electron microscope (SEM). The sample preparation and testing processes are shown in Figure 2.

For non-standard specimens with aggregate particle size ≤30 mm, according to the requirements of concrete test specifications, it is necessary to multiply the test value with a correction coefficient of 0.95 to obtain the true compressive strength of concrete. The accessing methods for the effect of rubber powder on the mechanical properties of HPC include:

(1) Compressive strength tests: Servo hydraulic universal testing machine was used to test the compressive strength and the loading rate was 0.4 MPa/s. The average value is used as the final strength value for this mixture.

The compressive strength of concrete is calculated as follows:

$$\sigma_c = F/A \tag{1}$$

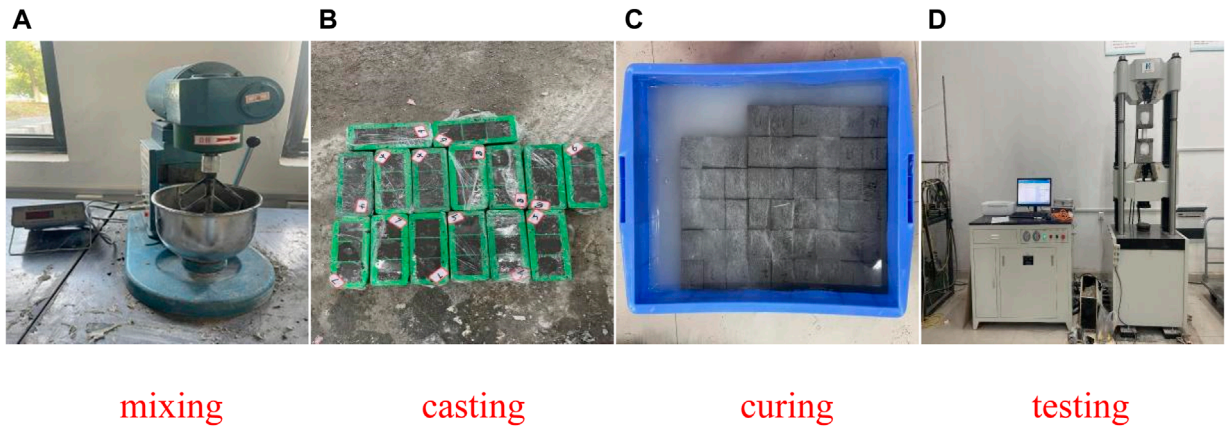


FIGURE 2
Sample preparation and testing.

where: $\sigma_c$—axial compressive strength of rubber concrete (MPa), $F$—failure load value of the specimen (N), A—bearing surface area of the specimen ($mm^2$).

(2) Splitting tensile strength tests: The RMT servo pressure testing machine was used to perform the splitting tensile test on the disc specimens and the average value was used as the final strength value under the mixture. The test was controlled by displacement, and the loading rate was 0.2 mm/min.

The splitting tensile strength of concrete is calculated as follows:

$$\sigma_t = 2P_t/\pi DL \quad (2)$$

where: $P_t$—what is the load of failure; L—Specimen length; D—Diameter of the specimen;

(3) Microstructural analysis: German ZEISS195 ULTRA 55 Type Field Emission Scanning Electron Microscope was used to analyze the microstructure of concrete fracture section. The specific production steps of the sample are as follows:
   a. In each experimental group, concrete specimens with an age of 28 days were selected, and the size of the specimens was about 1 cm with a side length of about 1 cm and a flat surface of sheet cement blocks.
   b. Add an appropriate amount of alcohol and seal it in a sealed bag, soak it overnight, and number it.
   c. After the samples are removed the next day, vacuum treatment is carried out for 24 h using a vacuum pump.
   d. After the vacuum treatment is completed, the sample is resealed into a new sealed bag.
   e. Electron microscope scanning.

# 4 Experimental results and discussion

## 4.1 Compressive strength

The static uniaxial compression test of HPC and HPRC specimens was carried out by using a universal testing machine, and the average compressive strength values of HPC and HPRC were calculated according to Eq. 1, as shown in Table 3.

TABLE 3 Compressive test results of HPRC and HPC (MPa).

| Group number | 3d | 7d | 28d |
|---|---|---|---|
| HPC | 34.8 | 60.7 | 80.8 |
| HPRC-10%–10% | 30.3 | 55.2 | 62.5 |
| HPRC-10%–20% | 24.9 | 47.2 | 61.1 |
| HPRC-10%–30% | 21.6 | 41.9 | 52.6 |
| HPRC-20%–10% | 30.3 | 55.5 | 66.0 |
| HPRC-20%–20% | 28.6 | 47.8 | 61.99 |
| HPRC-20%–30% | 26.9 | 42.3 | 57.5 |
| HPRC-30%–10% | 37.5 | 56.0 | 66.1 |
| HPRC-30%–20% | 32.9 | 52.2 | 62.4 |
| HPRC-30%–30% | 25.6 | 46.5 | 62.0 |

The findings presented in Table 3 reveal varying degrees of decrease in the compressive strength of concrete (HPRC) upon the incorporation of different amounts and particle sizes of rubber powder into high-performance concrete (HPC). For instance, following 28 days of curing, the uniaxial compressive strength of HPC measures at 80.8 MPa, whereas the corresponding maximum strength of HPRC is notably reduced to 66.1 MPa. Due to its elastic nature, the incorporation of rubber into cement-based materials results in a decrease in their strength. Furthermore, the hydrophobic nature of rubber surfaces leads to the presence of numerous minuscule pits on the particles' surface. Upon addition of rubber particles to mortar or concrete, the surface tension impedes water penetration into these pits. Consequently, the cement hydration product fails to effectively bond with the rubber particles. Upon

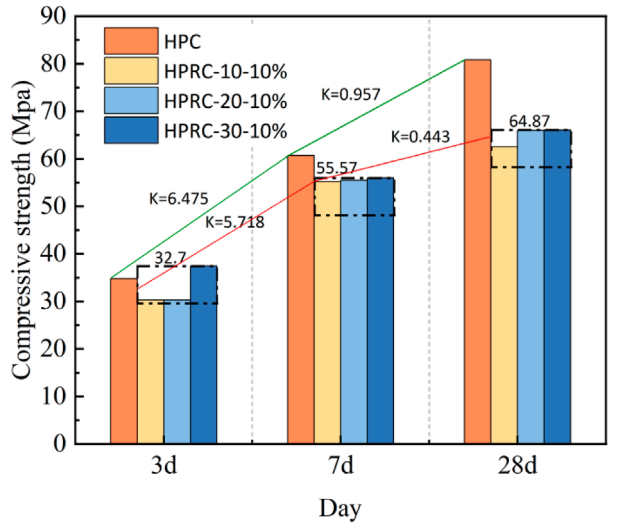


FIGURE 3
Uniaxial compressive strength of HPC and HPRC under different curing time.

hardening, significant pores form between the cement matrix and the rubber particles, exacerbating the weakening effect on the strength of the mortar or concrete.

Furthermore, the strength characteristics of HPC and HPRC exhibit distinct trends over varying curing durations, with the influence of rubber particle size and content on HPC strength demonstrating significant disparities. Accordingly, based on the comprehensive analysis of the test data presented in Table 3, this study delves into the effects of curing time, rubber particle size and dosage on the strength of HPC and HPRC.

By elucidating these interdependencies, the research endeavors to offer valuable insights into optimizing concrete formulations and enhancing the mechanical performance of rubber-modified high-performance concrete for practical engineering applications.

### 4.1.1 Variation of the compressive strength of HPC and HPRC with the curing time

The compressive strength values of HPC and HPRC (with a rubber content of 10%) from Table 3 were selected and plotted in Figure 3.

Analysis of Figure 3 indicates a positive correlation between the uniaxial compressive strength of both HPC and HPRC over time. Initially, when cured for 3 days, the compressive strength of HPRC stands at 32.7 MPa, while that of HPC is slightly higher at 34.8 MPa, demonstrating negligible disparity between the two. However, as curing progresses, the gap between the uniaxial compressive strength of HPC and the average compressive strength of HPRC with varying rubber particle sizes gradually widens. By the end of the 28-day standard curing period, the uniaxial compressive strength values of HPC and HPRC are 60.7 MPa and 55.57 MPa, respectively, reflecting a difference of nearly 16 MPa between the two materials.

Furthermore, the strength growth rate K is calculated for both HPC and HPRC across different curing time periods, as depicted in Figure 3. The strength growth rate K was defined as the strength difference divided by the curing time difference. For example, the curing time increased from 3 to 7 days, and the strength growth rate was calculated by:

$$K = \frac{S_7 - S_3}{D_7 - D_3}$$

where, K is the strength growth rate (MPa/day), S is the strength (MPa), and D is the curing time (days).

For instance, when the curing time extends from 3 to 7 days, the strength growth rate K for HPC is 6.475, while the corresponding rate for HPRC is 5.718. Similarly, as the curing time progresses from 7 to 28 days, the strength growth rate K for HPC reduces to 0.957, whereas the corresponding rate for HPRC decreases to 0.443. These findings suggest that in the initial curing period (within 3–7 days), the inclusion of rubber has minimal impact on HPC strength. Comparing the strength growth rates during this phase reveals that the internal hydration reaction of both HPC and HPRC predominantly determines their strength. However, beyond 7 days of curing (within 7–28 days), as the hydration reaction diminishes, rubber particles emerge as the primary factor influencing HPC strength. Analysis of the strength growth rates during this interval indicates that the incorporation of rubber particles results in a gradual increase in HPRC strength.

In concrete, cement undergoes hydration in the presence of water, forming a crystalline gel that enhances the material's strength. Initially, during the early stages of curing, the hydration reaction of cement proceeds at a slow pace, leading to comparable compressive strengths between HPC and HPRC. However, with prolonged curing time, the incorporation of rubber particles induces a greater increase in pores within the internal gel structure of HPRC compared to HPC. This results in a relatively weaker connection between the cement matrix, leading to a progressive divergence in strength between the two materials during the later stages of curing.

### 4.1.2 Influence of rubber particle size and content on the compressive performance of HPRC

In order to explore the influence of rubber particle size and dosage on the compressive strength of HPRC, the compressive strength data of HPRC specimens after curing for 28 days in Table 3 are plotted in Figure 5.

#### 4.1.2.1 Effect of rubber particle size

Figure 5 reveals that, at identical dosages, the strength of HPRC increases with decreasing rubber mesh number (i.e., smaller rubber particle size). For instance, when the rubber content is 10% (represented by the orange columnar bar in Figure 4), the strength of HPRC incorporating 20-mesh rubber surpasses that of 10-mesh rubber by 3.5 MPa, while HPRC incorporating 30-mesh rubber exhibits a further increase in strength compared to 10-mesh rubber, albeit by a smaller margin of 0.1 MPa. A similar trend is observed at rubber contents of 20% and 30%. These findings suggest that incorporating 20-mesh rubber results in the most substantial increase in HPRC strength, with diminishing gains as the rubber particle size decreases further.

Additionally, utilizing Figure 5, the HPRC strength growth rate K (defined as the strength difference divided by the rubber mesh difference) is calculated for various particle sizes. Specifically, when the rubber content is 10%, the strength growth rate K is 0.35 as the

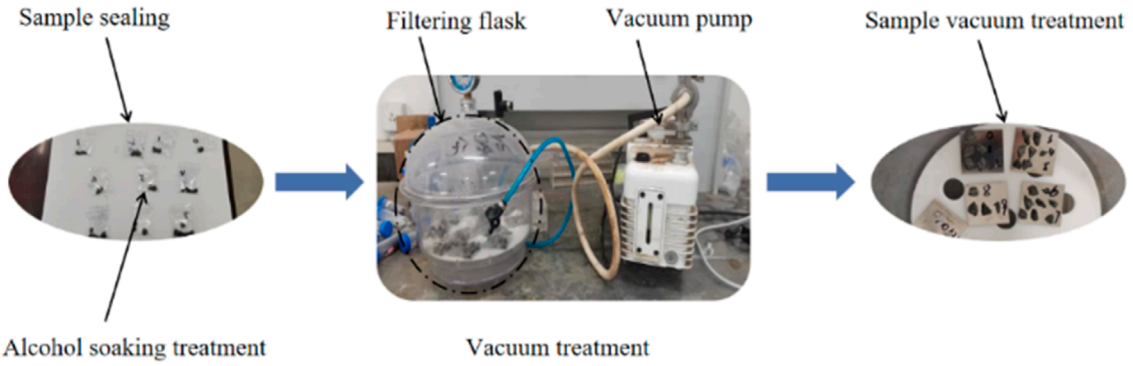


FIGURE 4
Sample preparation process.

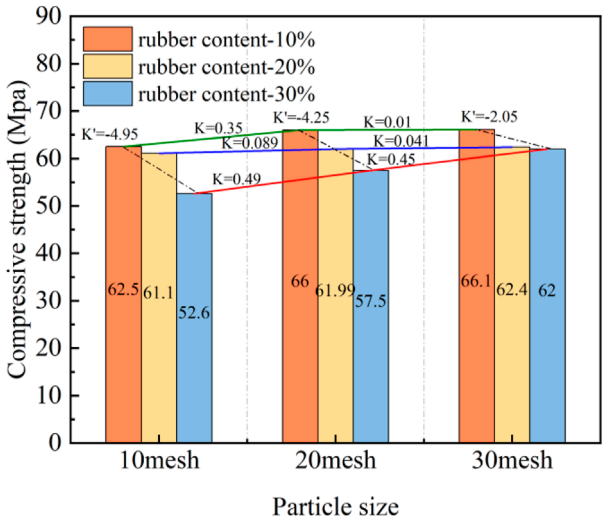


FIGURE 5
Uniaxial compressive strength of HPRC under different particle size and dosage.

rubber mesh number increases from 10 mesh to 20 mesh, and 0.01 as it increases from 20 mesh to 30 mesh. Similarly, for rubber contents of 20% and 30%, the strength growth rates K are (0.089, 0.041) and (0.49, 0.45), respectively. These calculations validate that the strength growth rate of HPRC slows down when transitioning from 20 mesh to 30 mesh rubber, particularly at lower rubber contents (10% and 20%). Furthermore, the second-stage K values of HPRC mixed with 10%, 20%, and 30% rubber are 0.01, 0.041, and 0.045, respectively, indicating that higher rubber contents correspond to greater strength growth rates of HPRC across different particle sizes. This suggests that the reduction in rubber particle size contributes significantly to the increase in HPRC strength, with larger K values indicating more pronounced strength enhancements.

#### 4.1.2.2 Effect of rubber content

Figure 5 illustrates a notable trend: the uniaxial compressive strength of HPRC declines gradually with increasing rubber content for a given mesh size of rubber particles. For instance, with 10-mesh rubber, the strength of HPRC diminishes by 1.4 MPa and 9.9 MPa as the rubber content escalates from 10% to 30%. Similarly, the relationship between HPRC strength and rubber content exhibits analogous characteristics for 20-mesh and 30-mesh rubber. Moreover, employing data from Figure 3, linear regression analysis was conducted on the strength of HPRC incorporating varying rubber contents under identical mesh sizes. This facilitated the derivation of the strength reduction rate $K'$ with increasing rubber content. Specifically, with 10-mesh rubber, the strength reduction rate $K'$ is −4.95 as the rubber content increases from 10% to 30%. Meanwhile, for 20-mesh and 30-mesh rubber, the strength reduction rates $K'$ are −4.25 and −2.05, respectively. Comparative analysis suggests that larger rubber particle sizes (e.g., 10 mesh) exhibit a more pronounced decline in HPRC strength with increasing rubber content. Conversely, for smaller rubber particle sizes (e.g., 30 mesh), the influence of increased rubber content on HPRC strength attenuation tends to diminish.

The experimental findings demonstrate a decrease in the uniaxial compressive strength of HPC upon the incorporation of rubber powder. This reduction can be attributed to several factors. Firstly, rubber particles consist of polymeric organic material and exhibit hydrophobic surfaces, leading to the formation of voids and pores at the interface between the cement slurry and rubber aggregate. This weakens the integrity of the concrete, consequently diminishing its strength. Additionally, the inclusion of rubber particles results in decreased fluidity of the concrete mixture, further exacerbating the formation of weak areas and compromising the material's strength. However, as the particle size of the incorporated rubber diminishes and approaches a powder-like form, the gap within the internal structure of HPC filled with rubber becomes exceedingly small, thereby mitigating the trend of strength decline.

## 4.2 Splitting tensile strength

The Brazilian splitting test was carried out on HPC and HPRC specimens by universal testing machine, and the average tensile strength values of HPC and HPRC were calculated according to Eq. 2, as shown in Table 4.

10.3389/fmats.2024.1426979

TABLE 4 Splitting tensile strength of HPRC and HPC (MPa).

| Group number | 3d | 7d | 28d |
|---|---|---|---|
| HPC | 1.814 | 3.728 | 5.055 |
| HPRC-10%–10% | 2.112 | 2.879 | 3.475 |
| HPRC-10%–20% | 2.076 | 2.588 | 4.290 |
| HPRC-10%–30% | 2.379 | 3.018 | 3.954 |
| HPRC-20%–10% | 2.348 | 3.242 | 4.301 |
| HPRC-20%–20% | 2.355 | 3.087 | 4.515 |
| HPRC-20%–30% | 2.199 | 3.281 | 4.174 |
| HPRC-30%–10% | 2.550 | 3.720 | 4.474 |
| HPRC-30%–20% | 3.043 | 3.727 | 4.571 |
| HPRC-30%–30% | 3.009 | 3.679 | 4.433 |

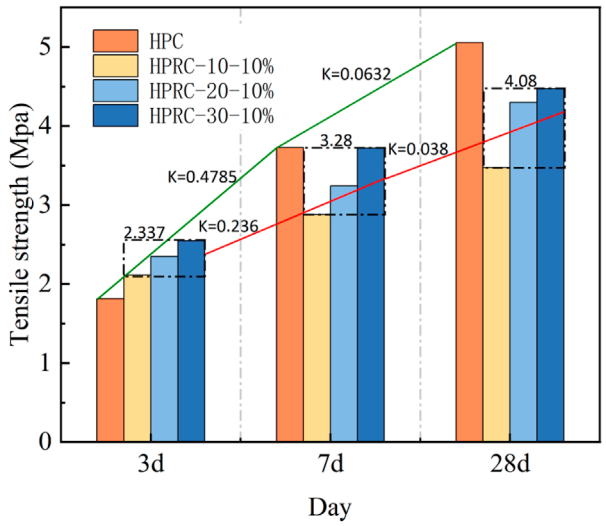


FIGURE 6
Uniaxial tensile strength of HPC and HPRC under different curing time.

Analysis of Table 4 reveals distinct patterns in the tensile strength of HPRC compared to its compressive strength when different amounts and particle sizes of rubber powder are incorporated into HPC. Notably, the uniaxial tensile strength of HPC is consistently lower than that of all HPRC variants after a 3-day curing period. However, for HPRC formulations containing rubber particles, tensile strength exhibits variability corresponding to changes in mesh number and rubber content. Consequently, leveraging the test data from Table 4, the impact of curing time, rubber particle size, and dosage on the tensile strength of both HPC and HPRC is comprehensively examined.

### 4.2.1 Variation of tensile strength of HPC and HPRC with curing time

The tensile strength values of HPC and HPRC with a rubber content of 10% in Table 4 are selected and plotted in Figure 6.

Figure 6 illustrates the progression of uniaxial tensile strength for both HPC and HPRC over different curing periods. Notably, the average tensile strength of HPRC with various rubber particle sizes surpasses that of HPC after 3 days of curing, with HPRC exhibiting a tensile strength of 2.337 MPa compared to HPC's 1.814 MPa. However, as curing time advances, the tensile strength of HPC exceeds that of HPRC after 7 days, with further widening of the disparity observed after 28 days of standard curing. This trend suggests that during the initial curing stages, the incorporation of rubber enhances the tensile strength of HPC. This phenomenon is attributed to the slower hydration reaction and subsequent strength development in the early stages, resulting in lower tensile strength for the benchmark concrete compared to rubber concrete.

Furthermore, the strength growth rate K (representing the difference in tensile strength divided by the difference in curing time) is computed for both HPC and HPRC across various curing periods, as depicted in Figure 6. Specifically, when the curing time extends from 3 to 7 days, the calculated tensile strength growth rate K for HPC is 0.478, while for HPRC, it is 0.236. Similarly, as the curing time progresses from 7 to 28 days, the tensile strength growth rate K for HPC and HPRC is determined as 0.0632 and 0.038, respectively.

As previously discussed, the initial stage of curing is characterized by a slow hydration reaction, leading to a gradual increase in tensile strength. Within this context, the presence of rubber particles embedded within HPRC serves to act as bridges during the specimen splitting process, thereby yielding a higher tensile strength compared to HPC. However, as the hydration reaction progresses, the deficiency in interfacial bonding between rubber particles and cement-based materials becomes evident, resulting in a consistently higher rate of tensile strength growth for HPC compared to HPRC.

### 4.2.2 Influence of rubber particle size and content on the tensile strength of HPRC

In order to explore the influence of rubber particle size and dosage on the tensile strength of HPRC, the tensile strength data of HPRC specimens after curing for 28 days in Table 4 are plotted in Figure 7.

#### 4.2.2.1 Effect of rubber particle size

Figure 7 illustrates that, holding dosage constant, the tensile strength of HPRC increases with a decrease in rubber mesh number, indicative of smaller rubber particle sizes. For instance, at a rubber content of 20%, the tensile strength of HPRC mixed with 20-mesh rubber exhibits a 0.225 MPa increase compared to that mixed with 10-mesh rubber. Similarly, transitioning from 20-mesh to 30-mesh rubber results in a comparable 0.225 MPa increase, with a marginal 0.056 MPa rise observed when progressing from 20-mesh to 10-mesh rubber. Analogously, at a rubber content of 10%, HPRC's tensile strength follows a similar trend concerning particle size, primarily manifesting between 10-mesh and 20-mesh rubber. Beyond this range, a diminution in rubber particle size fails to yield a significant increase in HPRC tensile strength.

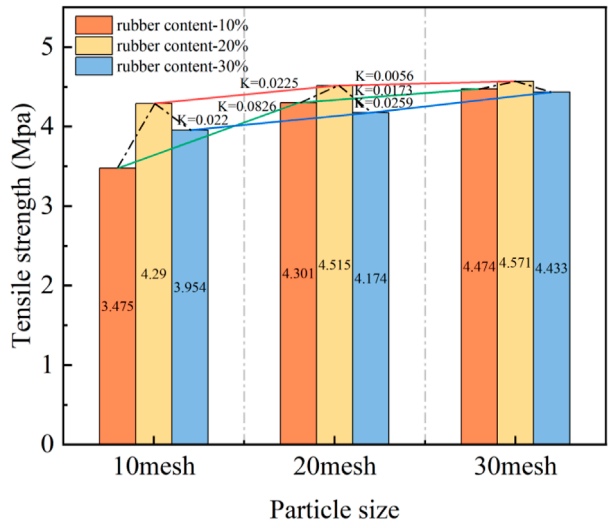


FIGURE 7
Uniaxial tensile strength of HPRC under different particle sizes and dosages.

Furthermore, the data from Figure 7 facilitates the computation of the HPRC tensile strength growth rate, denoted as K (strength difference/rubber mesh difference), across various particle sizes. For instance, at a rubber content of 10%, transitioning from 10-mesh to 20-mesh rubber yields a strength growth rate (K) of 0.0826, while the shift from 20-mesh to 30-mesh rubber corresponds to a reduced growth rate of 0.0173. Likewise, at rubber contents of 20% and 30%, the strength growth rates (K) are 0.0225 and 0.0056, respectively, for the 10-mesh to 20-mesh transition, and 0.022 and 0.0259, respectively, for the 20-mesh to 30-mesh transition. These findings underscore that the tensile strength growth rate of HPRC diminishes as rubber mesh number increases from 20 to 30, particularly evident at lower rubber contents (10% and 20%).

#### 4.2.2.2 Effect of rubber content

Figure 7 further reveals a noteworthy trend regarding the tensile strength of HPRC when mixed with rubber of identical particle size, illustrating a pattern of initial increase followed by decrease as dosage escalates. For instance, with 10-mesh rubber, a rise in rubber content from 10% to 20% results in a 0.815 MPa increase in HPRC tensile strength, which subsequently declines by 0.336 MPa upon further increase to 30%. Similar changing characteristics are observed for 20-mesh and 30-mesh rubber, wherein HPRC strength peaks at a rubber content of 20%. Notably, when the rubber particle size is larger (10 mesh), alterations in rubber content exert a more pronounced effect on enhancing or diminishing HPRC tensile strength. Conversely, with smaller rubber particle sizes (30 mesh), the impact of increasing rubber content on HPRC tensile strength modulation tends to diminish.

The foregoing analysis underscores a direct correlation between smaller rubber particle size and heightened tensile strength in HPRC. This relationship can be attributed to the diminutive size of rubber particles, which afford a substantial specific surface area conducive to fostering robust bonding with concrete, thereby augmenting tensile strength. Notably, when the rubber dosage reaches 20%, the tensile strength of HPRC reaches its zenith. This observation suggests that HPRC tensile strength is contingent not only upon the strength of the gel phase but also on the bridging effect facilitated by rubber particles. Thus, at a 20% dosage, the combined influence of these factors culminates in maximal tensile strength in HPRC.

## 4.3 Macro and micro damage analysis

### 4.3.1 Macro fracture modes of HPC and HPRC

During the initial loading phase, the HPC specimen exhibited minimal alterations. However, upon application of the load, a plethora of micro-cracks emerged throughout both the upper and lower regions of the specimen. Notably, during this phase, the data recorded by the testing apparatus continued to ascend. Upon reaching the limit of the specimen's load-bearing capacity, an abrupt, substantial oblique crack ensued accompanied by an audible sound, coinciding with a rapid decline in the testing machine's readings. Figure 8A illustrates the resultant damage to the HPC specimen.

Figure 8B depicts the resulting damage to the HPRC specimen. In the preliminary phase of loading, the HPRC specimen exhibits minimal change. Subsequent to this, small cracks begin to manifest in the test piece, accompanied by a continuous shattering sound. With further increases in load, the number of cracks in the specimen proliferates, and the width of these cracks expands. Ultimately, the specimen reaches its load-bearing limit, culminating in failure, while the testing machine readings decrease gradually and evenly. Findings indicate that under uniaxial pressure, the failure mode of high-performance concrete surpasses that of ordinary concrete, demonstrating robust resistance to deformation under axial pressure.

Upon comparing the morphological analysis of damage between HPC and HPRC as depicted in the figure, notable distinctions emerge. Unlike the HPC specimen, the HPRC specimen exhibits fewer instances of brittle and extensive cracks. Instead, a higher incidence of small cracks is observed, characterized by interruptions in their propagation during the diffusion process, ultimately resulting in enhanced integrity upon failure. This phenomenon is more pronounced with increased rubber particle content. Such observations primarily stem from alterations in the physical composition of the cement matrix following the incorporation of rubber powder. The introduction of fine elastic rubber particles enhances the interface between the aggregate and the cement matrix, thereby mitigating the detrimental effects on the cement matrix. Consequently, the initiation and propagation of cracks are effectively suppressed, yielding notable differences in damage morphology between the two materials. Moreover, the prevalence of interrupted cracks can be attributed to the intrinsic deformability of rubber, which impedes crack development within the concrete. Consequently, these cracks exhibit increased resistance to penetration, thereby maintaining better integrity upon failure.

### 4.3.2 Microfracture morphology of HPRC

At the mesoscopic level, initial defects such as larger pores and aggregate particles are discernible. The coupling effect between cement mortar and coarse and fine aggregate particles represents

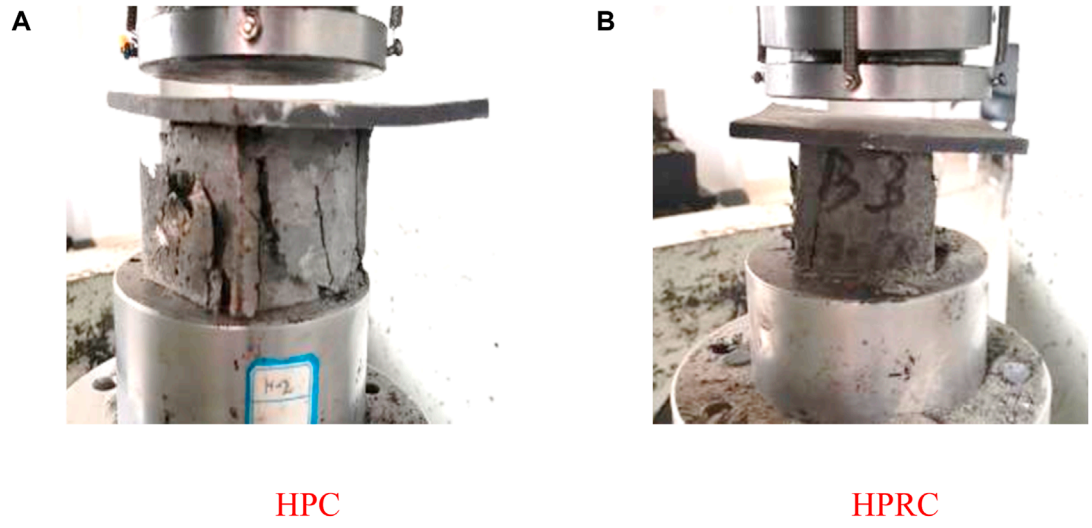


FIGURE 8
Macroscopic failure diagrams of HPC and HPRC specimens.

a fundamental characteristic of concrete. The heterogeneity observed in concrete materials stems from stress concentration resulting from the non-uniformity of the internal microstructure, consequently leading to a reduction in macroscopic strength. Thus, investigating initial defects at the mesoscopic scale facilitates a more comprehensive understanding of the fundamental principles governing concrete damage and failure evolution.

Given that the bonding area between rubber particles and the HPC matrix material represents the weakest link within the entire system, this study scrutinizes the surface morphology of HPRC blended with rubber particles of varying sizes, alongside the morphology of the interface between rubber particles and the cementing material matrix. The scanning electron microscope (SEM) images are presented in Figure 9.

Figure 9 reveals the morphological characteristics of the HPRC cross-section under magnifications ranging from 200 to 5,000 times. The cross-section exhibits distinct features, including the cementitious material matrix, rubber particles, micropores, and the interface between rubber particles and the cementitious material matrix. Notably, an evident gap exists between the rubber particles and the cementitious material matrix in HPRC. This phenomenon arises from the presence of hydrophobic substances and other impurity phases on the surface of the rubber particles, which diminishes the interfacial bonding strength between the two components.

Upon closer examination, it is evident that HPRC sections blended with 10-mesh rubber display numerous micropores and cracks between the rubber particles and the cementitious material matrix. In contrast, HPRC sections mixed with 20-mesh rubber still contain micropores, albeit with reduced gaps between the rubber particles and the cementitious material matrix. Furthermore, HPRC sections incorporating 30-mesh rubber primarily exhibit gaps between the rubber particles and the cementitious material matrix.

These observations indicate that as the rubber particle size decreases, the prevalence of micropores within HPRC diminishes, while the gaps between rubber particles and the cementitious material matrix shrink, thereby substantially improving the interface bonding condition.

The observed reduction in rubber particle size can be attributed to a diminished air-entraining effect, consequently leading to a decrease in pores within HPRC. Concurrently, the decrease in volume and increase in specific surface area of rubber particles facilitate enhanced bonding with concrete, thereby augmenting the interfacial bonding strength between the cementitious material matrix and rubber particles. This improvement in interfacial bonding strength contributes to the enhanced mechanical properties of HPRC.

## 5 Conclusion

Based on the principle of preparing ultra-high performance concrete, rubber particles were used instead of fine aggregates to prepare HPRC. The effect of rubber particle size and content on the mechanical properties of HPRC was studied, and the mechanism of the effect of rubber particles on the mechanical properties of HPRC was revealed through microscopic analysis. The main conclusions are as follows:

(1) With the decrease of rubber particle size, the compressive strength and tensile strength of rubber concrete show an increasing trend, that is, the particle size weakening effect. Under the condition of the same particle size of rubber particles, the compressive strength decreases gradually with the increase of the dosage, while the tensile strength increases first and then decreases, and reaches the maximum at the dosage of 20%.

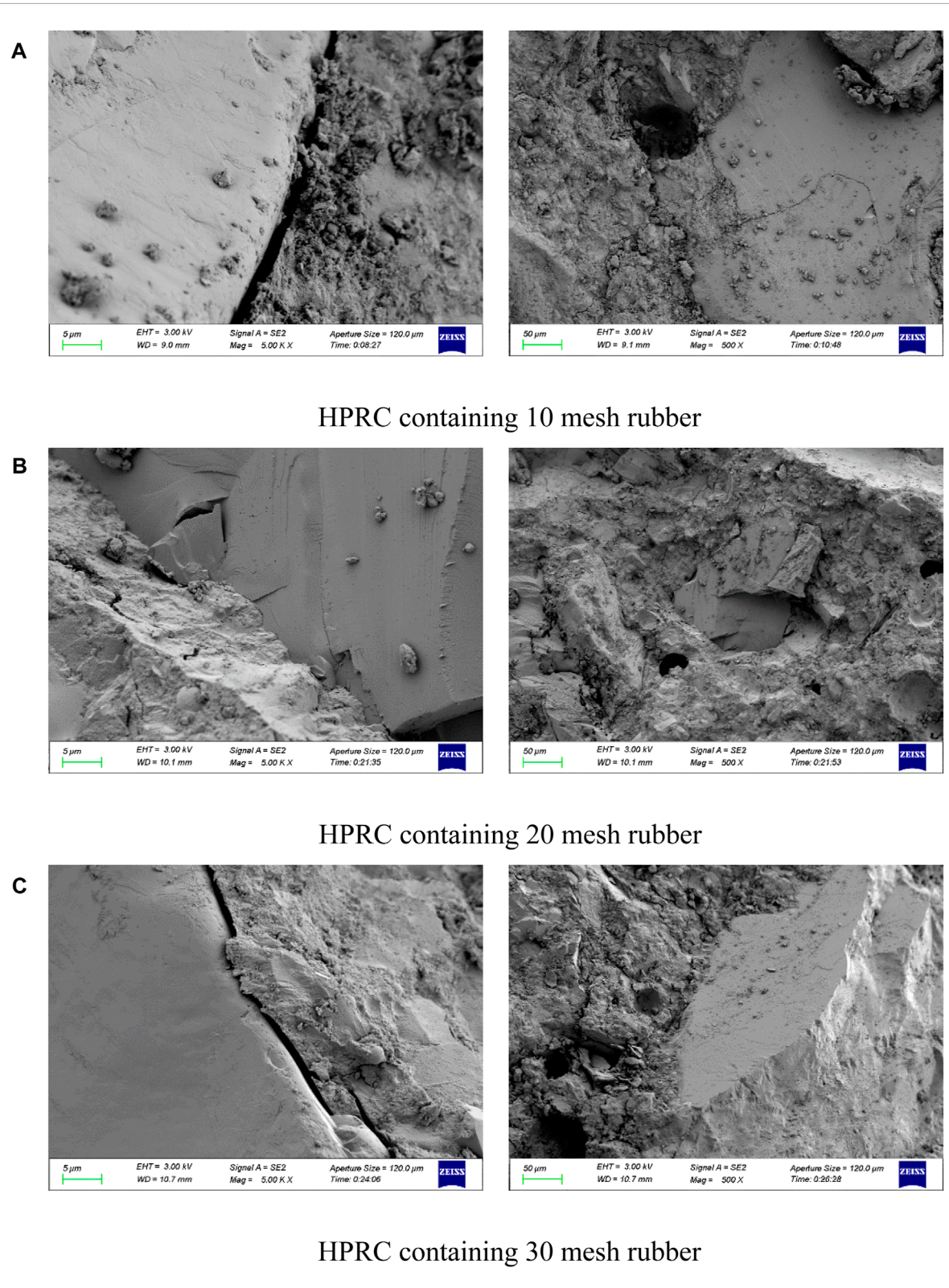


FIGURE 9
Microstructure characteristics of HPRC cross sections with different particle sizes at 30% content.

(2) From the point of view of the damage form, the right amount of rubber particles can make the concrete show the damage characteristics of brittleness and elongation.

(3) Based on the microscopic morphology, it can be found that the reduction of rubber particle size, that is, the reduction of volume and the increase of specific surface area, is conducive

to strengthening the bond with concrete, thus improving the interface bond strength between the gel material matrix and rubber particles.

(4) The test results show that high-performance rubber concrete has the potential to improve the durability and sustainability of construction projects, and the structure constructed with high-performance rubber concrete can withstand greater loads and impact forces. In addition, adding rubber to concrete can enhance its sustainability by incorporating recycled materials into construction practices. These findings contribute to a growing body of knowledge of innovative building materials and technologies to improve the efficiency and sustainability of the construction industry.

(5) Given the limited scope of this study, further research is needed to fully understand the static mechanical properties of high-performance rubber concrete. One suggestion for future research is to investigate the long-term durability of this material. This may involve conducting accelerated aging tests to simulate the effects of long-term exposure to environmental conditions such as freeze-thaw cycles and chemical degradation.

## Data availability statement

The original contributions presented in the study are included in the article/Supplementary Material, further inquiries can be directed to the corresponding author.

## Author contributions

JG: Funding acquisition, Writing–original draft, Writing–review and editing, Project administration, Supervision. GM: Investigation, Writing–review and editing. XG: Formal Analysis, Investigation, Writing–original draft. YX: Data curation, Formal Analysis, Writing–review and editing. SD: Data curation, Methodology, Writing–review and editing.

## Funding

The authors declare that financial support was received for the research, authorship, and/or publication of this article. This work was financially supported by the National Natural Science Foundation of China (No. 52104116).

## Conflict of interest

The authors declare that the research was conducted in the absence of any commercial or financial relationships that could be construed as a potential conflict of interest.

## Publisher's note



## References

Agrawal, D., Waghe, U., Ansari, K., Dighade, R., Amran, M., Qader, D. N., et al. (2023). Experimental effect of pre-treatment of rubber fibers on mechanical properties of rubberized concrete. *J. Mater. Res. Technol.* 23, 791–807. doi:10.1016/j.jmrt.2023.01.027

Al-Osta, M. A., Al-Tamimi, A. S., Al-Tarbi, S. M., Al-Amoudi, O. S. B., Al-Awsh, W. A., and Saleh, T. A. (2022). Development of sustainable concrete using recycled high-density polyethylene and crumb tires: mechanical and thermal properties. *J. Build. Eng.* 45, 103399. doi:10.1016/j.jobe.2021.103399

Bala, A., and Gupta, S. (2021). Thermal resistivity, sound absorption and vibration damping of concrete composite doped with waste tire Rubber: a review. *Constr. Build. Mater.* 299, 123939. doi:10.1016/j.conbuildmat.2021.123939

Cao, J., He, H., Zhang, Y., Zhao, W., Yan, Z., and Zhu, H. (2024). Crack detection in ultrahigh-performance concrete using robust principal component analysis and characteristic evaluation in the frequency domain. *Struct. Health Monit.* 23 (2), 1013–1024. doi:10.1177/14759217231178457

Cui, D., Wang, L., Zhang, C., Xue, H., Gao, D., and Chen, F. (2024). Dynamic splitting performance and energy dissipation of fiber-reinforced concrete under impact loading. *Materials* 17 (2), 421. doi:10.3390/ma17020421

Golewski, G. L. (2023a). Concrete composites based on quaternary blended cements with a reduced width of initial microcracks. *Appl. Sci.* 13 (12), 7338. doi:10.3390/app13127338

Golewski, G. L. (2023b). Study of strength and microstructure of a new sustainable concrete incorporating pozzolanic materials, Structural Engineering and Mechanics. *Int'l J.* 86 (4), 431–441. doi:10.12989/sem.2023.86.4.431

Golewski, G. L. (2023c). Effect of coarse aggregate grading on mechanical parameters and fracture toughness of limestone concrete. *Infrastructures* 8 (8), 117. doi:10.3390/infrastructures8080117

Golewski, G. L. (2023d). The phenomenon of cracking in cement concretes and reinforced concrete structures: the mechanism of cracks formation, causes of their initiation, types and places of occurrence, and methods of detection—a review. *Buildings* 13 (3), 765. doi:10.3390/buildings13030765

Golewski, G. L. (2024a). Investigating the effect of using three pozzolans (including the nanoadditive) in combination on the formation and development of cracks in concretes using non-contact measurement method. *Adv. Nano Res.* 16 (3), 217–229. doi:10.12989/sem.2023.86.4.431

Golewski, G. L. (2024b). Enhancement fracture behavior of sustainable cementitious composites using synergy between fly ash (FA) and nanosilica (NS) in the assessment based on digital image processing procedure. *Theor. Appl. Fract. Mech.* 131, 104442. doi:10.1016/j.tafmec.2024.104442

He, S., Jiang, Z., Chen, H., Chen, Z., Ding, J., Deng, H., et al. (2023). Mechanical properties, durability, and structural applications of rubber concrete: a state-of-the-art-review. *Sustainability* 15 (11), 8541. doi:10.3390/su15118541

Huang, H., Li, M., Yuan, Y., and Bai, H. (2022). Theoretical analysis on the lateral drift of precast concrete frame with replaceable artificial controllable plastic hinges. *J. Build. Eng.* 62, 105386. doi:10.1016/j.jobe.2022.105386

Huang, H., Yuan, Y., Zhang, W., and Li, M. (2021a). Seismic behavior of a replaceable artificial controllable plastic hinge for precast concrete beam-column joint. *Eng. Struct.* 245, 112848. doi:10.1016/j.engstruct.2021.112848

Huang, H., Yuan, Y., Zhang, W., and Zhu, L. (2021b). Property assessment of high-performance concrete containing three types of fibers. *Int. J. Concr. Struct. Mater.* 15, 39–17. doi:10.1186/s40069-021-00476-7

Juveria, F., Rajeev, P., Jegatheesan, P., and Sanjayan, J. (2023). Impact of stabilisation on mechanical properties of recycled concrete aggregate mixed with waste tyre rubber as a pavement material. *Case Stud. Constr. Mater.* 18, e02001. doi:10.1016/j.cscm.2023.e02001

Li, H., Yang, Y., Wang, X., and Tang, H. (2023) "Effects of the position and chloride-induced corrosion of strand on bonding behavior between the steel strand and concrete". *Structures*, 58. 105500. doi:10.1016/j.istruc.2023.105500

Long, X., Mao, M., Su, T., Su, Y. t., and Tian, M. k. (2023). Machine learning method to predict dynamic compressive response of concrete-like material at high strain rates. *Def. Technol.* 23, 100–111. doi:10.1016/j.dt.2022.02.003

Lu, D., Meng, F., Zhou, X., Zhuo, Y., Gao, Z., and Du, X. (2023). A dynamic elastoplastic model of concrete based on a modeling method with environmental factors as constitutive variables. *J. Eng. Mech.* 149 (12), 04023102. doi:10.1061/jenmdt.emeng-7206

Lu, D., Zhou, X., Du, X., and Wang, G. (2019). A 3D fractional elastoplastic constitutive model for concrete material. *Int. J. Solids Struct.* 165, 160–175. doi:10.1016/j.ijsolstr.2019.02.004

Luo, Y., Liao, P., Pan, R., Zou, J., and Zhou, X. (2024). Effect of bar diameter on bond performance of helically ribbed GFRP bar to UHPC. *J. Build. Eng.* 91, 109577. doi:10.1016/j.jobe.2024.109577

Medina, D. F., Martínez, M. C. H., Medina, N. F., and Hernández-Olivares, F. (2023). Durability of rubberized concrete with recycled steel fibers from tyre recycling in aggresive enviroments. *Constr. Build. Mater.* 400, 132619. doi:10.1016/j.conbuildmat.2023.132619

Mohseni, E., and Koushkbaghi, M. (2023). Recycling of landfill waste tyre in construction materials: durability of concrete made with chipped rubber. *Constr. Build. Mater.* 409, 134114. doi:10.1016/j.conbuildmat.2023.134114

Roychand, R., Gravina, R. J., Zhuge, Y., Ma, X., Mills, J. E., and Youssf, O. (2021). Practical rubber pre-treatment approch for concrete use—an experimental study. *J. Compos. Sci.* 5 (6), 143. doi:10.3390/jcs5060143

Sambucci, M., Marini, D., and Valente, M. (2020). Tire recycled rubber for more eco-sustainable advanced cementitious aggregate. *Recycling* 5 (2), 11. doi:10.3390/recycling5020011

Shahzad, K., and Zhao, Z. (2022). Experimental study of NaOH pretreated crumb rubber as substitute of fine aggregate in concrete. *Constr. Build. Mater.* 358, 129448. doi:10.1016/j.conbuildmat.2022.129448

Siahkouhi, M., Li, C., Astaraki, F., Rad, M. M., Fischer, S., and Jing, G. (2022). Comparative study of the mechanical behavior of concrete railway sleeper mix design, using waste rubber and glass materials. *Acta Polytech. Hung.* 19 (6), 213–224. doi:10.12700/aph.19.6.2022.6.15

Singaravel, D. A., Veerapandian, P., Rajendran, S., and Dhairiyasamy, R. (2024). Enhancing high-performance concrete sustainability: integration of waste tire rubber for innovation. *Sci. Rep.* 14 (1), 4635. doi:10.1038/s41598-024-55485-9

Valente, M., Sambucci, M., Chougan, M., and Ghaffar, S. H. (2023). Composite alkali-activated materials with waste tire rubber designed for additive manufacturing: an eco-sustainable and energy saving approach. *J. Mater. Res. Technol.* 24, 3098–3117. doi:10.1016/j.jmrt.2023.03.213

Wang, H., and Pang, J. (2023). Mechanical properties and microstructure of rubber concrete under coupling action of sulfate attack and dry–wet cycle. *Sustainability* 15 (12), 9569. doi:10.3390/su15129569

Wei, J., Ying, H., Yang, Y., Zhang, W., Yuan, H., and Zhou, J. (2023). Seismic performance of concrete-filled steel tubular composite columns with ultra high performance concrete plates. *Eng. Struct.* 278, 115500. doi:10.1016/j.engstruct.2022.115500

Yao, X., Lyu, X., Sun, J., Wang, B., Wang, Y., Yang, M., et al. (2023). AI-based performance prediction for 3D-printed concrete considering anisotropy and steam curing condition. *Constr. Build. Mater.* 375, 130898. doi:10.1016/j.conbuildmat.2023.130898

Youssf, O., Swilam, A., and Tahwia, A. M. (2023). Performance of crumb rubber concrete made with high contents of heat pre-treated rubber and magnetized water. *J. Mater. Res. Technol.* 23, 2160–2176. doi:10.1016/j.jmrt.2023.01.146

Zhang, H., Gao, M., Feng, Y., and Lv, L. (2023). Volume stability study of new low-clinker high performance concrete. *Case Stud. Constr. Mater.* 18, e02068. doi:10.1016/j.cscm.2023.e02068